

Infrared remote sensing of Mars and the Mars astrobiology exploration strategy

Laurel E. Kirkland^a, Kenneth C. Herr^b, John W. Salisbury^c, Eric R. Keim^b,
Paul M. Adams^b, and John A. Hackwell^b

^aLunar and Planetary Institute, 3600 Bay Area Blvd., Houston, TX 77058, kirkland@lpi.usra.edu

^bThe Aerospace Corp., P.O. Box 92957, Los Angeles, CA 90009

^cJohns Hopkins University, *retired*, 84 Cochise Ct., Palm Coast, FL 32137

ABSTRACT

The Mars exploration strategy calls first for the detection from orbit of minerals indicative of environments conducive to the support of life or the preservation of biomarkers. That information would then be used for astrobiology landing site selection. The near-term search will be conducted by the 1996 Global Surveyor Thermal Emission Spectrometer (TES) and the 2001 Mars Odyssey 9-band radiometer Thermal Emission Imaging System (THEMIS). This places the productivity of TES and THEMIS in the critical path of the Mars astrobiology strategy. Most predictions of mineral detection limits for TES and THEMIS are based on laboratory spectra of fresh mineral surfaces. However, standard laboratory measurements of fresh mineral surfaces generally do not reproduce all the spectral effects of weathering and surface roughness that are very apparent in field spectra, and these differences can critically affect interpretations of TES and THEMIS data. Here we examine causes of variations in spectral contrast, and differences in spectral signatures recorded in the field and in typical laboratory measurements, and show what the results indicate for the search for minerals and landing sites using TES and THEMIS. We conclude that for TES and THEMIS to attain their predicted mineral detection limits, minerals must be present under specific conditions: well-crystalline, smooth-surfaced at several scales, and low atmospheric downwelling radiance contribution. As a result, TES and THEMIS should not necessarily be used to exclude landing sites that are of interest for other reasons (e.g. geomorphology), but that exhibit no clear detections of minerals of interest to astrobiologists.

Keywords: Mars, infrared remote sensing, astrobiology, TES, THEMIS, SEBASS

1. INTRODUCTION

The current Mars exploration strategy calls first for orbited infrared spectral instruments to identify locations with key minerals to provide data for geologic and climatic interpretations, and to determine the most favorable landing sites to explore for a Martian fossil record and sample return [e.g. Christensen et al., 1992, Carr et al., 1994; Farmer and Des Maris, 1999]. It was expected that TES (~5.7–50 μm) would detect and identify the minerals present. This would be followed by more detailed spatial mapping at low spectral resolution using the 2001 nine-band radiometer THEMIS (6.8–12.6 μm).

Christensen et al. [2000a, 2000b] conclude that TES has recorded the signature of surface silicates and hematite. However, TES has been less productive than hoped in locating definitive signatures of deposits of key minerals such as carbonates and sulfates, although these materials are predicted to be present, and TES was expected to be able to detect them [Christensen et al., 1992]. Current explanations for the puzzling lack of detections include that the materials were never there; that they are buried [McKay and Nedell, 1988]; altered by UV radiation [Mukhin, et al., 1996]; occur exclusively in small deposits (exposed over less than one-tenth of the TES ~3 km x 5 km field of view) [Kerridge, 1997; Farmer and Des Maris, 1999]; or that they are rough and weathered, and so exhibit low spectral contrast [Kirkland et al., 2000a,b]. If Mars had a denser CO₂ atmosphere in its past and if liquid water had been present on its surface, then large deposits of carbonate materials likely formed [Pollack et al., 1987]. Thus the lack of carbonate detections in TES data affects interpretations of the geologic and climatic history of Mars. It may also affect the choice of landing sites.

In remote sensing studies, it is important to note the difference between *detection*, *discrimination*, and *identification*. Detection requires a spectral signal that rises to a statistically meaningful level above the noise level; discrimination requires the spectral signal be detectable and also different from the surrounding materials; and identification requires

both discrimination and a spectral band shape that can be considered unambiguous and that can be converted to an appropriate unit for comparison to laboratory measurements for identification. For example, remotely sensed spectra may be converted to apparent emissivity [Conel, 1969] and compared to laboratory spectra scaled in emissivity [Kahle and Alley, 1992], which is the typical approach for TES studies [e.g. Christensen et al., 200a,b].

Christensen et al. [1992, p.7725] state that the scientific foundation for TES surface interpretations rests mainly on laboratory spectral studies combined with studies using the airborne multi-channel radiometer TIMS (Thermal Infrared Multispectral Scanner), which has 6 bands in the ~8–12 μm region. Almost all airborne terrestrial thermal infrared studies have focused on multi-channel radiometer (multi-spectral) data sets, typically with four to ten bands. Kahle et al. [1993] and Hook et al. [1999] present good reviews, and representative instruments include TIMS [Kahle and Goetz, 1983; Gillespie et al., 1984; Abrams et al., 1991]; the Moderate Resolution Imaging Spectroradiometer (MODIS) Airborne Simulator (MAS) [King et al., 1996]; the MODIS/ASTER airborne simulator (MASTER) [Hook et al., 2001]; and on the Terra satellite, the Moderate Resolution Imaging Spectroradiometer (MODIS) [Barnes et al., 1998], the Advanced Spaceborne Thermal Emission and Reflection Radiometer (ASTER) [Fujisada and Ono, 1991].

An important drawback inherent in using less than ~10 bands is that such instruments lack the spectral resolution to measure the direct, diagnostic signature of most minerals and rocks, except quartz and some silicates [Crowley and Hook, 1996]. However, under some conditions materials with narrow or weak features may be statistically differentiated from surrounding regions based on an overall difference in emissivity or continuum, the lack of a silicate feature, or broad inflections that are not uniquely diagnostic, and then the targets are subsequently identified using ground truth, commonly using laboratory spectra [e.g. Kahle and Rowan, 1980; Gillespie et al., 1984; Gillespie et al., 1986; Gillespie, 1992; Crowley and Hook, 1996]. Thus for non-silicates, TIMS studies typically use statistical techniques to define spectral type regions in the TIMS image, and then identify the type region materials using ground truth. This "TIMS+ground-truth+lab"-style approach has been used with great success to map terrestrial surface mineralogy.

A search of the literature returned no peer-reviewed studies that made extensive use of airborne thermal infrared imaging spectrometer (hyperspectral) data. In part, this results from the high data rate required of an imaging spectrometer, the difficulty in obtaining high signal-to-noise ratio (SNR) from narrower bands, and the ability to combine statistical differentiation of type regions with ground truth to identify the minerals present.

However, given the heavy reliance on ground truth for the "TIMS+ground-truth+lab" studies, they leave one important, relatively unstudied question in the chain of remote sensing testing: How do thermal-infrared hyperspectral signatures measured from an airborne or satellite platform compare to laboratory signatures typically used for interpretation? Since (until recently) no airborne, imaging thermal emission spectrometer existed that measures with a sensitivity broadly comparable to laboratory spectra, this question had to remain relatively untested.

Since a multi-spectral instrument cannot identify most minerals without benefit of ground-truth, TES was designed as a hyperspectral instrument, able to measure 143 or 256 bands over ~5.7–50 μm (1750–200 cm^{-1}). The approach selected next was for TES to identify the minerals present, and then THEMIS would provide higher spatial resolution mapping of the previously identified minerals.

The spectral library used for TES team interpretations contains measurements of crushed, sieved (710–1000 μ), washed samples [Christensen et al., 2000c]. If a laboratory spectrum of a fresh mineral surface exhibits a strong band that is not observed in TES spectra, then it is concluded that the mineral is not present at the ~10% level [Christensen et al., 2000a, 2000b]. In order for this method to produce accurate interpretations, fresh and weathered surfaces must exhibit the same band depth, and materials with the same composition must always weather to produce the same surface roughness, regardless of the internal microstructure. To examine the effects of weathering on mineral spectra and interpretations of field spectra using laboratory spectra of fresh surfaces, we used very high signal-to-noise ratio, hyperspectral terrestrial data measured by the airborne Spatially Enhanced Broadband Spectrograph System (SEBASS, 7.6–13.5 μm , 128 channels; Hackwell et al., 1996). SEBASS provides the unprecedented capability to move the hyperspectral testing for TES interpretations from the laboratory into the field environment; to examine weathering effects over a much broader range of samples than is possible with laboratory samples alone; and to characterize effects not commonly reproduced in

the laboratory environment. We also measured *in situ* spectra using field spectrometers (6.68–14.28 μm), and laboratory spectra (2.5–200 μm) of field samples collected with the *in situ* upper surface marked for comparison to the field data.

These spectral data sets were measured specifically to obtain an improved understanding of the variations in hyperspectral behavior between field hyperspectral signatures and standard laboratory spectra commonly used to interpret field data. We also desired to determine whether a "TIMS+ground-truth+lab" terrestrial analog study reproduces all spectral behavior that would significantly impact TES and THEMIS interpretations.

Here we focus on an assessment of how well and under what conditions carbonates may be detected, and under what conditions they may be identified using instruments such as TES and THEMIS, with a specific focus on the conditions required to detect and identify carbonates without benefit of ground truth. The field site studied is the Mormon Mesa, Nevada [Kirkland et al., 2000a,b]. Kirkland et al. [2001a] discuss this study in detail as applied to terrestrial remote sensing, and Keim et al. [2001] discuss SEBASS measurements of other regions. In the thermal infrared, calcite has clearly discernable bands centered near 6.5, 11.2, and 33 μm (890, 1540, 300 cm^{-1}). Our field work focuses on the 11.2 μm band because it falls within the terrestrial atmospheric $\sim 8\text{--}12$ μm window, but our laboratory studies include an examination of the 6.5 and 33 μm bands. In TES spectra, the calcite 11.2 and 33 μm bands are roughly equally detectable, and the 6.5 μm band is the least detectable [Kirkland et al., 2001b]. Insufficient details have been released on THEMIS to determine which band will be most detectable by it.

2. DATA SETS

TES. At the heart of TES is a Michelson interferometer spectrometer that measures from $\sim 5.7\text{--}50$ μm and with a spatial resolution of ~ 3 km x 5 km [Christensen et al., 1992]. Table 1 gives instrument details. TES has most commonly returned spectra containing 143 discrete measurements over a range of ~ 1470 cm^{-1} , and records one measurement every 10.58 cm^{-1} . In this mode, TES has a mirror throw of 0.25 mm and 20 cm^{-1} spectral resolution (unapodized), measured as the first zero crossing of the sinc response function. Figure 1 shows the TES SNR at 20 cm^{-1} resolution [Kirkland et al., 2001b]. TES also has a "5 cm^{-1} sampling mode," with better spectral resolution and 286 measurements per spectrum.

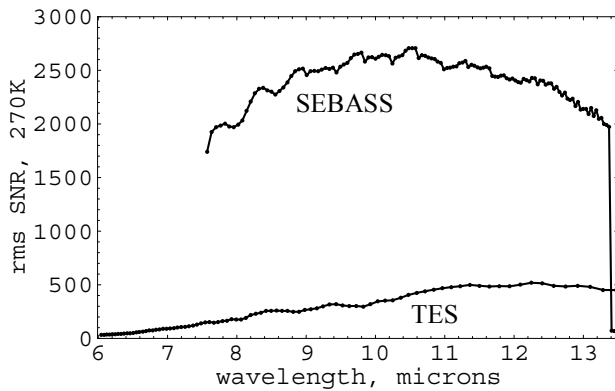


Figure 1: SNR. SEBASS (upper) and TES root mean square (rms) signal-to-noise ratio (SNR) over 6–13.5 μm for a 270K blackbody. Higher numbers represent greater sensitivity. For both instruments the rms SNR is approximately five times larger than the peak-to-peak SNR.

Table 1: Instrument parameters.

| instrument | 11 μm SNR ^a | 11 μm resolution ^b , cm^{-1} | channels ^c | wavelength range, μm ^d |
|--------------------------|-----------------------------------|---|-----------------------|--|
| 1996 TES ^e | 500 | 20.0 | 143 | $\sim 6\text{--}50$ |
| 2001 THEMIS ^f | $\sim 33\text{--}150$ | 90.0 | 8 ^d | 6.8–12.6 |
| SEBASS | 2500 | 7.4 | 128 | 7.6–13.5 |
| TIMS ^g | | | 6 | 8.4–11.6 |
| MASTER ^h | | | 10 | 7.8–12.9 |

^aSNR = 270K rms signal-to-noise ratio; ^bunapodized spectral resolution; TES also measures at 10 cm^{-1} resolution, but there are relatively few measurements at that resolution; ^cbands measured per spectrum; ^dValues at band centers. THEMIS also measures a ~ 15 μm band for atmospheric studies, but it does not sense the surface; ^e[Christensen et al., 1992]; ^f[Christensen et al., 1999]; ^g[Crowley and Hook, 1996]; ^hThermal-infrared channels, Hook et al., 2001.

TES spectra exhibit poorly understood behavior at the long wavelengths (Figure 2) that may be caused by a calibration issue, variations in the atmospheric aerosol dust, or another unknown cause. Possible calibration problems include stray light and uncertainties in the internal blackbody calibration target signature. Until the cause of the behavior can be better understood, we exclude the $\sim 18\text{--}50\ \mu\text{m}$ ($550\text{--}200\ \text{cm}^{-1}$) region, but the methods described here can be applied to any region where the continuum shape is well understood.

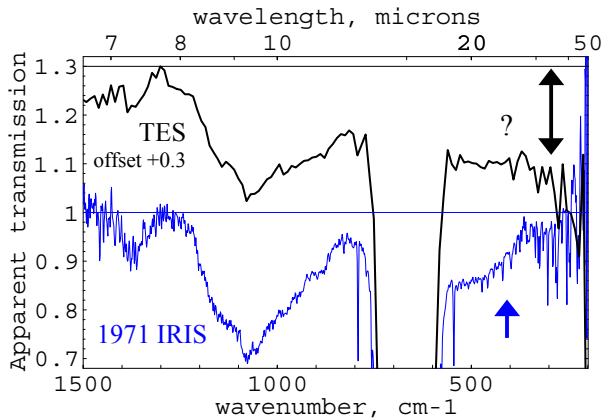


Figure 2: TES at long wavelengths. The 1971 Mariner Mars Infrared Interferometer Spectrometer (IRIS) spectrum shows the ubiquitous aerosol silicate bands centered near ~ 9 and $20\ \mu\text{m}$ (lower arrow). TES spectra exhibit a very similar broad $9\ \mu\text{m}$ band. However, in contrast to IRIS, TES spectra exhibit a more sloping continuum toward longer wavelengths and lower values in the $\sim 30\text{--}50\ \mu\text{m}$ region (upper, double arrow), and lack a well-defined $20\ \mu\text{m}$ band (lower arrow).

THEMIS. The Thermal Emission Imaging System has 8 bands with a band full width at half maximum of $\sim 0.9\text{--}1.2\ \mu\text{m}$ centered near $6.8, 7.9, 8.6, 9.4, 10.3, 11.1, 11.9, 12.6\ \mu\text{m}$ to measure the surface, and one band near $15\ \mu\text{m}$ for atmospheric sounding. Thus THEMIS is broadly comparable to TIMS, with the exception that THEMIS can measure to slightly shorter wavelength due to the lower atmospheric water vapor content of the Martian atmosphere, and it measures with poorer spectral resolution. Christensen et al. [1999] give the spatial resolution for THEMIS of $100\ \text{m}$, and an rms signal-to-noise ratio range of $33\text{--}150$, but the wavelength and target temperature are not specified. Figure 3 shows an example TES and SEBASS spectrum, and a THEMIS spectrum simulated from TES.

SEBASS. The Aerospace Corporation operates SEBASS under the direction of John Hackwell. SEBASS recorded very high quality hyperspectral images of Mormon Mesa in May, 1999 and September, 2000, covering $2.4\text{--}5.3$ and $7.6\text{--}13.5\ \mu\text{m}$, with a spectral resolution of $7.4\ \text{cm}^{-1}$ at $11\ \mu\text{m}$ (defined as two times the sampling interval), and a spatial resolution of ~ 1 or $2\ \text{m}$ (Table 1). SEBASS measures with the highest signal-to-noise ratio of any terrestrial airborne thermal infrared imaging spectrometer. Hackwell et al. [1996] give additional details. Figure 1 shows the SEBASS signal-to-noise ratio for a 270K blackbody target, calculated using the method described in Kirkland et al. [2001b], and Figure 3 shows an example spectrum of a region with near 100% coverage by indurated carbonate (calcrete).

An airborne survey provides an excellent analog to measurements from an orbited instrument. SEBASS covers the full terrestrial thermal infrared atmospheric window, measuring $7.6\text{--}13.5\ \mu\text{m}$, while TES measures $\sim 6\text{--}50\ \mu\text{m}$. In order to test the validity of interpreting remotely sensed hyperspectral signatures by comparison to laboratory spectra of fresh, smooth surfaces, it is essential that both TES and SEBASS measure remotely sensed field spectra in an overlapping thermal infrared range, and that both are spectrometers rather than multi-channel radiometers (e.g. TIMS, MASTER).

Field spectrometer. High quality field spectra covering $6.68\text{--}14.28\ \mu\text{m}$ were acquired using a van-mounted Brunswick Model 21 interferometer spectrometer that measures with $3.4\ \text{cm}^{-1}$ spectral resolution (apodized). Field spectrometers have the advantage that they view the target through a shorter atmospheric path length and can focus on specific targets for more in-depth measurements, and they allow a more detailed examination of the reduced spectral contrast caused by reflected downwelling radiance, which Kirkland et al. [2001a] discuss for the Mormon Mesa study. They also provide a cross-check for the airborne spectra. The field spectrometer data used here measured $\sim 0.3\ \text{m} \times 0.3\ \text{m}$ pixel size.

Laboratory. Reflectance measurements were made with a Nicolet Magna 550 Fourier transform infrared (FTIR) spectrometer equipped with a DTGS detector. Biconical reflectance spectra ($2.5\text{--}200\ \mu\text{m}$) were recorded with a Harrick

Scientific "praying mantis" diffuse reflectance attachment, using a Labsphere Infragold standard as the background spectrum. A solid substrate beamsplitter was used to record spectra from 9–200 μm , and a KBr beamsplitter from (2.5–25 μm). The 9–25 μm overlap region allowed spectra from both regions to be scaled if bands existed in the overlap region. Hemispherical reflectance measurements (2.5–25 μm) were made with a 3" diameter Labsphere integrating sphere lined with Infragold to determine absolute emissivity via Kirchhoff's Law (emissivity = 1- reflectance). The hemispherical spot size is 5 mm x 5 mm.

The upward facing weathered sample surfaces (as marked in the field) were examined to better correlate laboratory spectra with field spectra. In order to identify the major phases present, selected samples were analyzed by X-ray diffraction (XRD). The carbonate contents of samples were determined by gravimetric acid digestion. Hydrochloric acid insoluble residues were filtered, dried and weighed to determine the weight percentages of non-carbonate. The surfaces of the samples (both as-weathered and polished cross sections vacuum impregnated and mounted in epoxy) were examined by scanning electron microscopy (SEM) and chemically characterized by energy dispersive X-ray spectroscopy (EDXS). After coating with a thin conductive layer of carbon, samples were examined at 15 kV in a Hitachi S2500 SEM equipped with a KEVEX Delta EDXS system.

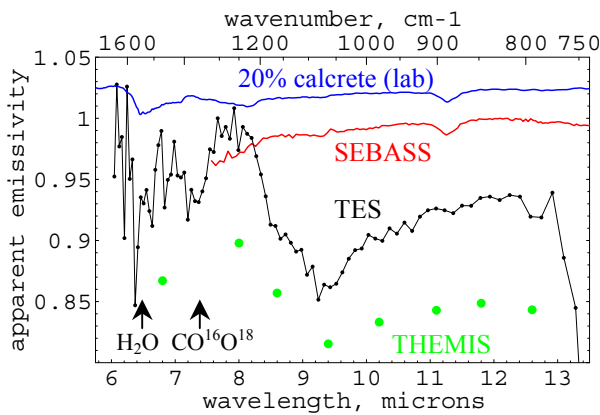


Figure 3: Example spectra. The THEMIS spectrum is simulated from the typical TES spectrum shown, but the lower SNR of THEMIS is not accounted for here. The SEBASS spectrum is of Mormon Mesa, and the lab spectrum is of calcrete (discussed in Section 4) simulating 20% coverage, and carbonate causes the 11.2 μm band. TES spectrum 57023856, from the NASA-PDS archive, converted to apparent emissivity with respect to the brightness temperature at 7.75 μm , 270K. The THEMIS spectrum is offset -0.1 and lab $+0.12$ for clarity. Transmission through the silicate aerosol dust is the main contributor to the broad ~ 9 μm TES band; CO_2 the 9.4 and 12.6 μm bands and the sharp ~ 13 μm drop-off; and arrows mark two other gas bands.

3. SPECTRAL CONTRAST

If minerals are exposed on the surface but not seen by TES, then this means they do not exhibit sufficient spectral contrast for TES to detect them. Surface properties unrelated to composition reduce spectral contrast [e.g. Lyon, 1964; Vincent and Hunt, 1968; Hunt and Logan, 1972; Salisbury et al., 1987; Salisbury and Wald, 1992; Kahle et al., 1988; Ramsey and Fink, 1999; Fabbri et al., 2001]. Most important are roughness that causes a cavity (hohlraum) effect, and particle size and roughness on a scale that causes volume scattering.

Cavity effect. Figure 4 shows the increase in effective emissivity (ϵ_e) with the number of reflections (*count*) off a cavity wall with true emissivity ϵ [LaRocca, 1978; Williams and Becklund, 1984; Fraden, 1993]:

$$\epsilon_e = 1 - (1 - \epsilon)^{(\text{count} + 1)} \quad (1)$$

Cavities (e.g. vesicles, pits between pebbles, interstices between grains, cracks and grooves in rocks) will cause a cavity effect and reduced spectral contrast according to Equation 1. Harloff and Arnold [2001] provide a simplified illustration of the effect in the near-infrared, and Thomas and King [1977] review general methods for surface roughness characterization.

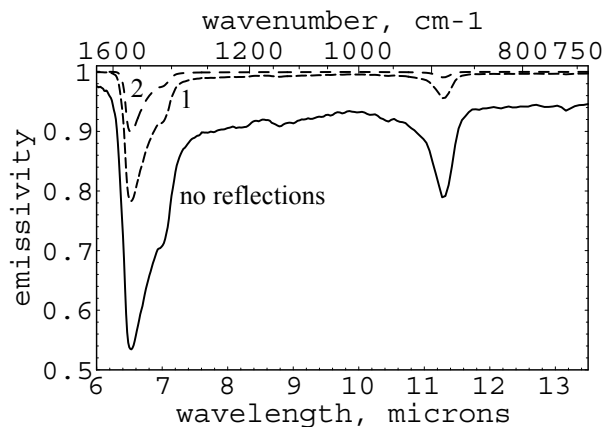


Figure 4: Cavity effect. The lower solid trace shows the measured spectrum of a fresh surface of a limestone hand sample, converted to emissivity using 1- hemispherical reflectance. The middle trace simulates one reflection, and the upper, dashed trace two reflections using Equation 1.

Surface and volume scattering. The spectra in Figure 5a were measured in biconical reflectance, and all other laboratory spectra shown here were measured in hemispherical reflectance, including spectra in Figure 5b–d, and converted to emissivity using one minus reflectance (Kirchhoff's Law). A Fresnel reflection from the surface is termed *surface scattering*. Surface scattering dominates for coarse particles, so the strong bands (called reststrahlen bands) in Figure 5a appear as emissivity troughs (spectral minima). In contrast, volume scattering results when particles are small enough to be optically thin, or where surface roughness is at a scale where rough edges are also optically thin. Volume scattering dominates the transmission spectrum, so the transmission bands are offset slightly toward longer wavelength than the reststrahlen bands, and appear as emission peaks. Increased volume scattering in the fine calcite spectrum causes reduced spectral contrast and a lowered continuum emissivity as it shifts to appear more as the transmission spectrum (Figure 5a).

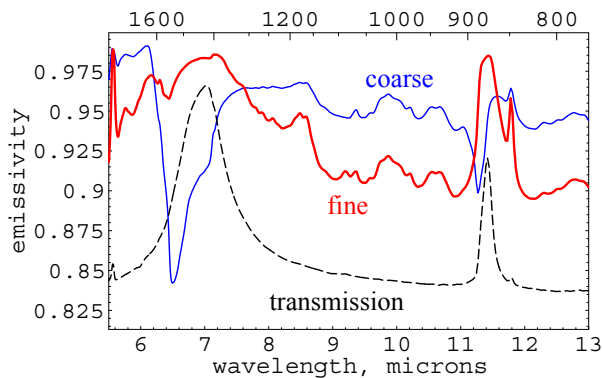


Figure 5a: Volume scattering. The dashed line shows a calcite transmission spectrum; the thick trace a biconical reflectance spectrum of fine calcite particles (0–74 μ), and the thin trace coarse calcite particles (74–250 μ). Spectra are from Salisbury et al., [1991], sample "calcite.1," using emissivity = 1 - biconical reflectance (or transmission), with transmission scaled to plot in a convenient range for display. Note that increased volume scattering decreases the continuum emissivity, which is the opposite trend to the cavity effect.

Figure 5b shows calcite spectra measured of three particle size ranges. A comparison of the spectra of 125–500 μ and 45–125 μ particle sizes shows that at this spectral resolution, volume scattering clearly affects the shape of the 11.2 μ band before the 6.5 μ reststrahlen band contrast has decreased greatly.

Figure 5c shows spectra measured of a limestone hand sample from Mormon Mesa [Kirkland et al., 2000a,b, 2001a]. The spectra are of (1) the upper, weathered surface; (2) a fresh surface; and (3) a surface that was saw cut, ground with a coarse grinding wheel, grit blasted with coarse Al_2O_3 , and then cleaned in an ultrasonic cleaner. The grit-blasted spectrum exhibits volume scattering effects in the lower continuum emissivity and altered 6.5 and 11.2 μ band shapes. This indicates the grit blasting causes micro-cracking and fracturing of the material on the surface. Figure 5d illustrates in more detail the altered shape of the 11.2 μ band caused by volume scattering that occurs before the 6.5 μ band depth is greatly reduced (Figure 5c). Relative to the fresh limestone surface, the weathered limestone surface shows no clear alteration of the 6.5 and 11.2 μ reststrahlen band shapes, but it exhibits reduced spectral contrast and a higher continuum emissivity. This indicates a cavity effect from surface roughness is the main contributor to the observed reduction in spectral contrast in the weathered vs. fresh surface.

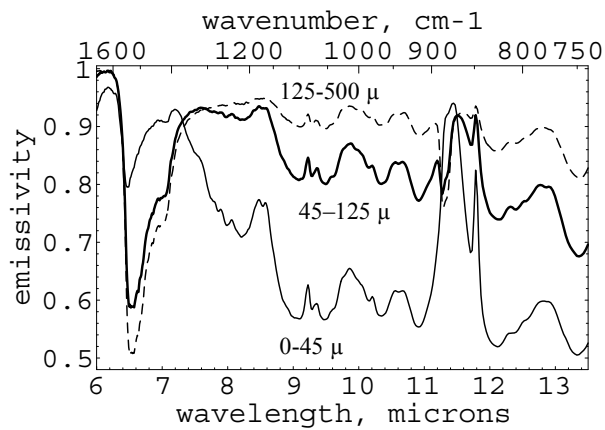


Figure 5b: Volume scattering. This shows calcite spectra measured for three particle size ranges as labeled. These spectra illustrate the decrease in reststrahlen band contrast and decrease in continuum emissivity with decreasing particle size. Spectra are from the ASTER online archive, sample "calcitec3e," using emissivity = 1 - hemispherical reflectance.

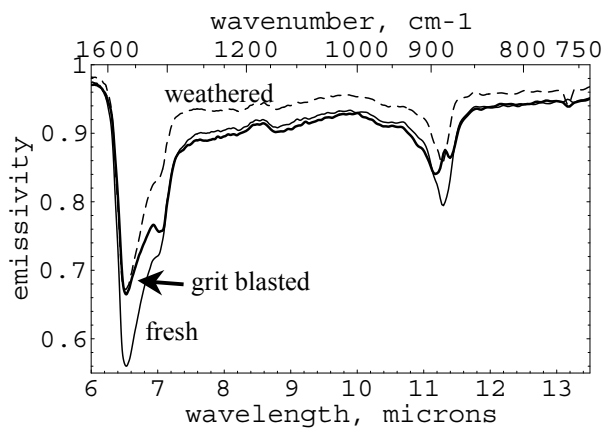


Figure 5c: Volume scattering vs. cavity effect. Relative to the fresh limestone surface, the grit-blasted surface shows altered spectral band shape and slightly lower continuum emissivity, consistent with volume scattering. The weathered surface exhibits no clear alteration of the band shapes, and has higher continuum emissivity and reduced spectral contrast, consistent with a cavity effect. (Sample 4-12C).

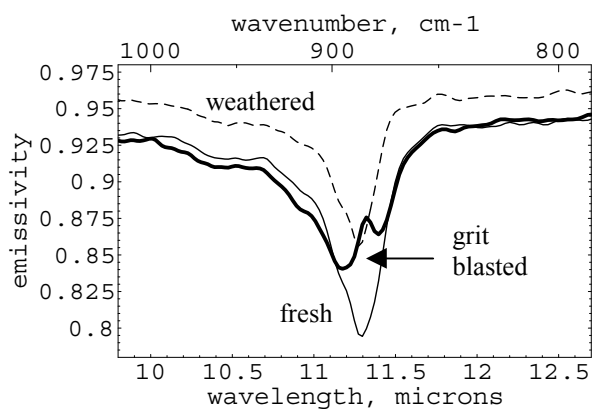


Figure 5d: Close-up of 11.2 μm region. This illustrates additional details of 11.2 μm band behavior shown in Figure 5c. Note the weathered surface exhibits reduced spectral contrast and higher emissivity relative to the fresh surface, but does not exhibit an altered band shape.

These spectra illustrate that a rough or particulate surface results in multiple scattering that will reduce the spectral contrast of reststrahlen bands due to the cavity effect, or volume scattering, or both. When measured with sufficient spectral resolution and SNR, if only one effect is mainly present, then which it is can be determined by comparison of the band shape and continuum emissivity to that of a large-particulate, smooth-surfaced sample. TES may have sufficient spectral resolution to make this determination, but it probably lacks the SNR to measure such subtle differences as in Figure 5c and 5d. THEMIS will not have the spectral resolution to differentiate between the band shapes illustrated in Figure 5c and 5d.

4. FIELD VS. LABORATORY SPECTRAL CONTRASTS

Figure 6 shows hyperspectral measurements from Mormon Mesa or samples collected from there [Kirkland et al., 2001a]. XRD measurements show the limestone is ~100% carbonate, mainly calcite, with minor amounts of dolomite. The indurated calcite (calcrete) is composed of ~90% calcite and ~10% quartz, as determined by XRD and gravimetric acid digestion. Cross-section SEM images, EDXS measurements, and the spectral signature over the 2.5–50 μm range give no indication of a clay coating on the calcrete.

The Figure 6 limestone laboratory spectrum exhibits spectral contrast typical of those carbonates used by Christensen et al. [2000a,b] to set TES and THEMIS detection limits. The calcrete laboratory spectrum, on the other hand, exhibits greatly reduced spectral contrast relative to the limestone, despite the fact that both materials are predominantly carbonate and outcrop in the same Mormon Mesa environment. The band shape of the calcrete indicates a cavity effect is the dominant cause of its reduced spectral contrast. In massive materials, roughness that causes a cavity effect may be present on three broad scales: (1) pits between individual rocks in piles of pebbles, cobbles, or boulders; (2) rough, pitted rock surfaces at a scale that is visible by eye (~mm's to cm's), and (3) a rough surface at sizes less than ~1 mm that can be seen in SEM images but are not readily detectable by eye. The roughness scale may be comparable to the grain scale and to infrared wavelengths. Roughness continues to affect the spectral contrast down to a scale of at least ~one-fifth the wavelength [Siegel and Howell, 1968]. In the field, the calcrete displays all of these scales of surface roughness.

The field and SEBASS spectra exhibit reduced spectral contrast relative to the laboratory calcrete, even though calcrete filled nearly 100% of the instruments' field of view. This indicates a cavity effect at scales not reproduced by the laboratory hand sample (e.g. pits between rocks) contributes to the observed reduced spectral contrast. Thus spectra measured in the field may exhibit lower spectral contrast than spectra measured of hand samples in the laboratory. This has not been clearly evident in airborne multi-channel radiometer studies (e.g. TIMS, MASTER) because those instruments lack the spectral resolution to detect spectral behavior that becomes evident in hyperspectral measurements.

Reflected downwelling atmospheric radiance also reduces spectral contrast, because reststrahlen bands are reflectance maxima. This effect is minimal here (Figure 6), but is a significant effect for strong (i.e. high reflectance) bands, or spectral ranges with a higher atmospheric radiance contribution [Kirkland et al. 2001a].

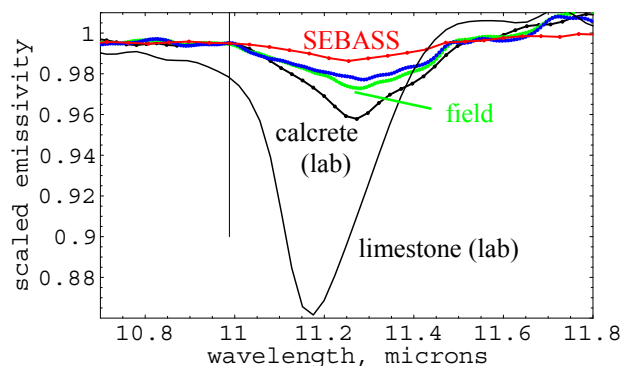


Figure 6: Field vs. lab spectral contrasts. Shown are laboratory spectra of limestone and calcrete (with lowest ~11.2 μm emissivity); a calcrete field spectrum that has been compensated (lower-middle) and not compensated (upper-middle) for reflected downwelling radiance, and a SEBASS spectrum (upper) of the same region measured by the field spectrometers. Lab spectra are converted to emissivity using 1-hemispherical reflectance, and the field spectra are in apparent emissivity. Field and SEBASS spectra are offset to match the SEBASS apparent emissivity at 10.99 μm (vertical reference line), and the limestone is offset +0.06.

5. SEARCHING FOR SPECTRAL FEATURES

It is sometimes assumed that the strongest band apparent in a laboratory spectrum will be the most detectable in a remotely sensed spectrum. For example, it is frequently assumed that the carbonate 6.5 μm band will be more detectable than the 11.2 μm band (e.g. Figure 3 and 5c). However, the signal-to-noise ratio of the remote sensing instrument usually varies with wavelength (e.g. Figure 1). As a result, a strong band that occurs in a low SNR region may or may not be as detectable as a weaker band measured in a region of high SNR.

Here we give an example calculation to determine whether the carbonate 6.5 or 11.2 μm band would provide the more sensitive detection in TES spectra. We use these two bands and carbonate as an example, but the method may be applied to any mineral or wavelength region where the continuum is well understood. The minimum band depth of a feature of unknown origin to accept as a detection is called the band detection limit (*DL*) and is given by [Kirkland et al., 2001b]:

$$DL = \frac{100 \times \text{Confidence Factor}}{\frac{\text{signal}}{\text{noise}_{ptop} / 2} \times \sqrt{\frac{\text{Band FWHM}}{\text{Sampling Interval}}}} \quad (2)$$

where DL = the minimum percent band depth required to accept as a detection; Confidence Factor = contrast relative to the peak-to-peak noise level a feature should exhibit to be accepted as real; signal = signal used in the SNR calculation; noise_{ptop} = peak-to-peak noise. The noise is divided by 2 to account for the measurement being made relative to the local continuum, so the deflection is referenced to one-half the peak-to-peak noise rather than the full peak-to-peak noise; Band FWHM = target band full width at the half maximum of the band depth; and Sampling Interval = spacing of points measured, which is 10.58 cm^{-1} for TES. The square root accounts for the increase in signal-to-noise that occurs with the square root of the number of points measured on the band; and the factor of 100 puts it on a percent scaling.

Figure 7 shows the band detection limit for TES for a band with $\text{FWHM}=30 \text{ cm}^{-1}$, and it illustrates the large variation with wavelength caused by the varying SNR. Table 2 gives the measured band depths and the TES band detection limit values for the 6.5 and 11.2 μm bands exhibited by a limestone and calcrete from Mormon Mesa. These band detection limits assume TES measures the material under similar conditions as those present for the laboratory measurement (the target surface is smooth for areas larger than the sample and fills the field of view, and no atmospheric effects). Atmospheric effects can be accounted for by an appropriate adjustment of the confidence factor.

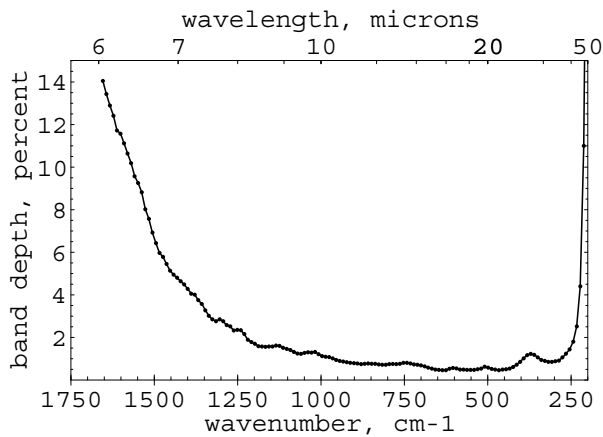


Figure 7: TES band detection limits. This shows the percent band depth required to accept as a detection, calculated using Equation 2, with $\text{FWHM}=30 \text{ cm}^{-1}$, and confidence factor=2. It shows the percent band depth that a feature must exhibit relative to the local continuum to be accepted as a detection. Higher numbers indicate a stronger spectral contrast is required for detection. It illustrates the variation in sensitivity with wavelength, and why linear mixture fits should be weighted by the varying SNR of the instrument.

Table 2: TES limestone and calcrete band detection limits, based on laboratory spectra measured of the upper weathered surface

| | limestone | calcrete |
|--|------------|------------|
| 11.2 μm (890 cm^{-1}) band width (cm^{-1}) | 40 | 30 |
| 11.2 μm (890 cm^{-1}) band depth | 14.2% | 4.8% |
| 11.2 μm (890 cm^{-1}) detection limit | 0.7% | 0.8% |
| 6.5 μm (1540 cm^{-1}) band width (cm^{-1}) | 118 | 110 |
| 6.5 μm (1540 cm^{-1}) band depth | 23.4% | 11% |
| 6.5 μm (1540 cm^{-1}) detection limit | 4.4% | 4.6% |
| detection limit ratio, 6.5:11.2 μm | 6.6 | 6.0 |
| band depth ratio, 6.5:11.2 μm | 1.6 | 2.3 |

where *detection limit ratio* is the ratio of the 1540 to the 890 cm^{-1} band detection limit; and *band depth ratio* is the ratio of the 1540 to 890 cm^{-1} band depths. Detection limits calculated for a confidence factor of 2.

For the limestone, Table 2 shows that because of the varying TES SNR with wavelength, the 6.5 μm band would need to have 6.6 times stronger contrast than the 11.2 μm band for it to be as detectable in TES spectra. However, the 6.5 μm band is only 1.6 times stronger. Thus for TES, the narrower, weaker 11.2 μm limestone band is actually more detectable than the stronger, broader 6.5 μm band. A similar result is obtained for the calcrete (Table 2). This critical but often overlooked point should be considered when determining and stating detection limits, and when searching a data base for mineral signatures. It would also be desirable to examine these effects for THEMIS, but its SNR as a function of wavelength and temperature remains proprietary.

6. SIGNIFICANCE

Whenever volume scattering or a cavity effect reduces the spectral contrast, that will reduce the ability of TES and THEMIS to detect minerals. If laboratory spectra measured of smooth, fresh hand sample surfaces (e.g. Figure 5c) or smooth, fresh, large particles (e.g. Figure 5b) of limestone were used to calculate the expected remotely sensed calcite band contrast, then we might use the remotely sensed Figure 6 SEBASS spectrum to conclude incorrectly that very little carbonate is present in a region that is in fact extensively covered by massive carbonates (Figure 8). Furthermore, if SEBASS measured with lower SNR or spectral resolution, it would not detect the 11.2 μm band, and we might conclude that no carbonates are present at all. The Mormon Mesa calcrete formed and weathered in a terrestrial environment, but it illustrates why the presence of rough and weathered surfaces must be considered to realistically predict detection limits and to reliably interpret remotely sensed spectra that have no accompanying ground truth.



Figure 8: Mormon Mesa. The indurated carbonate cap rock is marked for reference, and it is composed mainly of calcrete and a loamy, quartz-rich soil. Typical calcrete fragments are visible on the upper mesa surface. Also shown is the Aerospace Corporation's field spectrometer van.

Strong spectral contrast is consistent with a smooth surface with large, well-crystalline grains or a smooth-surfaced, glossy coating. Other than water ice and CO_2 ice, TES has recorded only one clear, reasonably diagnostic mineral signature, of hematite [Christensen et al., 2000a]. The dearth of strong surface mineral spectral signatures in TES data indicates that large exposures of smooth surfaces with well-crystalline minerals are very rare on Mars, as are smooth-surfaced regions with smooth coatings. Such materials should be easily detected if they are exposed over at least 10% of the TES $\sim 3 \text{ km} \times 5 \text{ km}$ field of view. The region exhibiting the hematite signature is a notable exception, and this indicates the presence of at least some smooth surfaces at this site. It also leads to the question of whether smooth coatings and minerals such as carbonates and sulfates are very rare on Mars, or whether smooth surfaces are rare.

The SEBASS spectra of Mormon Mesa show that deposits of massive, well-crystalline minerals may be present and remain undetected in TES and THEMIS data if sufficient surface roughness is present. However, SEBASS spectra clearly demonstrate that rough targets may be detected and identified using hyperspectral thermal infrared data with sufficiently high SNR.

If effects that reduce spectral contrast are not considered, then locations on Mars that do not exhibit mineral bands (e.g. carbonate, chert) in TES or THEMIS data may be ruled out as desirable landing sites even though minerals indicative of hot springs or other regions conducive to the support and preservation of life and biomarkers may in fact be present, as for example at Mormon Mesa. Thus while TES and THEMIS may be used to locate regions of interest, landing sites that appear interesting for other reasons (e.g. geomorphology) should not necessarily be excluded based on TES and THEMIS results. To improve understanding of these issues, laboratory studies should include measurements of weathered and rough surfaces, and field hyperspectral studies should be pursued in order to characterize significant effects not typically reproduced in laboratory studies, and to broaden the range of weathered samples measured.

7. REFERENCES

1. Abrams, M., E. Abbott, and A. Kahle, Combined use of visible, reflected infrared, and thermal infrared images for mapping Hawaiian lava flows, *J. Geophys. Res.* 96, 475-484, 1991.
2. Barnes, W. L., T. S. Pagano, V. V. Salomonson, Prelaunch characteristics of the Moderate Resolution Imaging Spectroradiometer (MODIS) on EOS-AM1, *IEEE Trans. on Geoscience and Rem. Sens.* 36, 1088-1100, 1998.
3. Carr, M. H. and 17 writing group members, *An Exobiological Strategy for Mars Exploration*, NASA SP-530, 1994.
4. Christensen, P. R., D. L. Anderson, S. C. Chase, R. N. Clark, H. H. Kieffer, M. C. Malin, J. C. Pearl, J. Carpenter, N. Bandiera, F. G. Brown, and S. Silverman, Thermal emission spectrometer experiment: Mars Observer mission, *J. Geophys. Res.* 97, 7719-7734, 1992.
5. Christensen, P. R., B. M. Jakosky, H. H. Kieffer, M. C. Malin, H. Y. McSween, K. Neelson, G. Mehall, S. Silverman, and S. Ferry, The Thermal Emission Imaging System (THEMIS) instrument for the Mars 2001 Orbiter, in *Workshop on Mars 2001: Integrated Science in Preparation for Sample Return and Human Exploration*, Houston, Oct. 2-4, LPI Contribution No.991, 28-30, 1999.
6. Christensen, P. R., and the TES team, Detection of crystalline hematite mineralization on Mars by the Thermal Emission Spectrometer: Evidence for near-surface water, *J. Geophys. Res.* 105, 9632-9642, 2000a.
7. Christensen, P. R., J. L. Bandfield, M. D. Smith, V. E. Hamilton, R. Clark, Identification of a basaltic component on the Martian surface from Thermal Emission Spectrometer data, *J. Geophys. Res.* 105, 9609-9621, 2000b.
8. Christensen, P. R. and the TES team, A thermal emission spectral library of rock-forming minerals, *J. Geophys. Res.* 105, 9735-9739, 2000c.
9. Conel, J. E., Infrared emissivities of silicates: Experimental results and a cloudy atmosphere model of spectral emission from condensed particulate mediums, *J. Geophys. Res.* 74, 1614-1634, 1969.
10. Crowley, J. K. and S. J. Hook, Mapping playa evaporite minerals and associated sediments in Death Valley, California, with multispectral thermal infrared images, *J. Geophys. Res.* 101, 643-660, 1996.
11. Fabbri, M., M. Picollo, S. Porcinai, and M. Bacci, Mid-infrared fiber-optics reflectance spectroscopy: A non-invasive technique for remote analysis of painted layers. Part I: Technical set-up, *Appl. Spec.* 55, 420-427, 2001.
12. Farmer, J. D. and D. J. Des Marais, Exploring for a record of ancient Martian life, *J. Geophys. Res.* 104, 26,977-26,995, 1999.
13. Fraden, J., *AIP Handbook of Modern Sensors*, p.136, AIP, New York, New York, 1993.
14. Fujisada, H. and A. Ono, Overview of ASTER design concept, in *Future European and Japanese Remote-Sensing Sensors and Programs*, 1-2 April 1991, Orlando, Florida – Proceedings of the SPIE Vol. 1490, P. Slater, Ed., Society of Photo-Optical Instrumentation Engineers, Bellingham, Washington, 244-254, 1991.
15. Gillespie, A. R., Spectral mixture analysis of multispectral thermal infrared images, *Rem. Sens. Environ.* 42, 137-145, 1992.
16. Gillespie, A. R., A. B. Kahle, and F. D. Palluconi, Mapping alluvial fans in Death Valley, California, using multichannel thermal infrared images, *Geophys. Res. Lett.* 11, 1153-1156, 1984.
17. Gillespie, A. R., A. B. Kahle, and R. E. Walker, Color enhancement of highly correlated images. I. Decorrelation stretch, *Rem. Sens. Environ.* 20, 209-235, 1986.
18. Hackwell, J. A., D. W. Warren, R. P. Bongiovi, S. J. Hansel, T. L. Hayhurst, D. J. Mabry, M. G. Sivjee, and J. W. Skinner, LWIR/MWIR Imaging Hyperspectral Sensor for Airborne and Ground-Based Remote Sensing, *Imaging Spectrometry II*, Proceedings of the International Soc. for Optical Eng., Vol. 2819, 102-107, 1996.
19. Harloff, J. and G. Arnold, Near-infrared reflectance spectroscopy of bulk analog materials for planetary crust, *Planet. and Space Sci.* 49, 191-211, 2001.
20. Hook, S. J., E. A. Abbott, C. Grove, A. B. Kahle, and F. Palluconi, Use of multispectral thermal infrared data in geological studies, Ch. 2 in *Remote Sensing for the Earth Sciences: Manual of Remote Sensing*, 3rd ed. Vol. 3, A. N. Rencz editor, 59-110, 1999.
21. Hook, S. J., J. J. Myers, K. J. Thome, M. Fitzgerald, and A. B. Kahle, The MODIS/ASTER airborne simulator (MASTER)--A new instrument for earth science studies, *Rem. Sens. of Environ.* 76, 93-102, 2001.
22. Hunt, G. R. and L. M. Logan, Variation of single particle mid-infrared emission spectrum with particle size, *App. Op.* 11, 142-147, 1972.
23. Kahle, A. B. and L. C. Rowan, Evaluation of multispectral middle infrared aircraft images from lithologic mapping in the east Tintic Mountains, Utah, *Geology* 8, 234-239, 1980.
24. Kahle, A. B. and A. F. H. Goetz, Mineralogical information from a new airborne thermal infrared multispectral scanner, *Science* 222, 24-27, 1983.

25. Kahle, A. B., A. R. Gillespie, E. A. Abbott, M. J. Abrams, R. E. Walker, G. Hoover, and J. P. Lockwood, Relative dating of Hawaiian lava flows using multispectral thermal infrared images: A new tool for geologic mapping of young volcanic terranes, *J. Geophys. Res.* 93, 15,239–15,251, 1988.
26. Kahle, A. B. and R. E. Alley, Separation of temperature and emittance in remotely sensed radiance measurements, *Remote Sens. Environ.* 42, 107–111 1992.
27. Kahle, A. B., F. D. Palluconi, and P. R. Christensen, Thermal emission spectroscopy: Application to the Earth and Mars, Ch.5 in *Remote Geochemical Analysis: Elemental and Mineralogical Composition*, C. Pieters and P. Englert ed., Cambridge UP, 1993.
28. Keim, E. R., L. E. Kirkland, J. A. Hackwell, and K. C. Herr, Terrestrial airborne hyperspectral remote sensing (SEBASS): Applications to remote sensing studies of Mars, *LPSC XXXII, abs. 2162*, also available on-line at www.lpi.usra.edu, 2001.
29. Kerridge, J. F., An exobiological strategy for Mars exploration, *LPI Tech. Rep. 97-01*, 15–19, 1997.
30. King, M. D. and the MAS instrument team, Airborne scanning spectrometer for remote sensing of cloud, aerosol, water vapor, and surface properties, *J. Atmospheric. and Oceanic Technology* 13, 777–794, 1996.
31. Kirkland, L. E., K. C. Herr, E. R. Keim, J. W. Salisbury, J. A. Hackwell, A Field Study of Thermal Infrared Spectra of Carbonates, with Implications for Studies of Mars, *LPSC XXXI, abs. 1876*, also available on-line at www.lpi.usra.edu, 2000a.
32. Kirkland L. E., K. C. Herr, P. M. Adams, J. W. Salisbury, and A. Treiman, A Laboratory Study of Weathered Carbonates, with Implications for the Infrared Remote Sensing of Carbonates on Mars, *LPSC XXXI, abs. 1915*, also available on-line at www.lpi.usra.edu, 2000b.
33. Kirkland, L. E., K. C. Herr, E. R. Keim, P. M. Adams, J. W. Salisbury, J. A. Hackwell, A. Treiman, First Use of an Airborne Thermal Infrared Hyperspectral Scanner for Compositional Mapping, submitted *Remote Sens. Environ.*, 2001a.
34. Kirkland, L. E., K. C. Herr, and J. W. Salisbury, Band Detection Limits in Thermal Infrared Spectra, accepted to *Applied Optics* and scheduled for publication Sept. 20, 2001b.
35. Lane, M. D. and P. R. Christensen, Thermal infrared emission spectroscopy of anhydrous carbonates, *J. Geophys. Res.* 102, 25,851–25,592, 1997.
36. LaRocca, A. J., Artificial Sources, Ch.2 in *The Infrared Handbook*, W. Wolfe and G. Zissis ed., ERIM Press, 1978.
37. Lyon, R. J. P., Evaluation of Infrared Spectrophotometry for Compositional Analysis of Lunar and Planetary Soils, Part 2, *NASA CR-100*, 1964.
38. McKay, C. P. and S. Nedell, Are there carbonate deposits in the Valles Marineris, Mars?, *Icarus* 73, 142–148, 1988.
39. Mukhin, L. M., A. P. Koscheev, Y. P. Dikov, J. Huth, and H. Wänke, Experimental simulations of the photodecomposition of carbonates and sulphates on Mars, *Nature* 379, 141–143, 1996.
40. Pollack, J. B., J. F. Kasting, S. M. Richardson, and K. Poliakoff, The case for a wet, warm climate on Early Mars, *Icarus* 71, 203–224, 1987.
41. Ramsey, M. S. and J. H. Fink, Estimating silicic lava vesicularity with thermal remote sensing: A new technique for volcanic mapping and monitoring, *Bull. Volcanol* 61, 32–39, 1999.
42. Salisbury, J. W., B. Hapke, and J. W. Eastes, Usefulness of weak bands in midinfrared remote sensing of particulate planetary surfaces, *J. Geophys. Res.* 92, 702–710, 1987.
43. Salisbury, J. W., L. S. Walter, N. Vergo, D. M. D’Aria, *Infrared (2.1-25 μ m) Spectra of Minerals*, Johns Hopkins UP, Baltimore, 1991.
44. Salisbury, J. W. and A. Wald, The role of volume scattering in reducing spectral contrast of reststrahlen bands in spectra of powdered minerals, *Icarus* 96, 121–128, 1992.
45. Siegel, R. and J. Howell, Thermal Radiation Heat Transfer Vol. 1, *NASA SP-164*, 1968.
46. Thomas, T. R. and M. King, *Surface Topography in Engineering: A State of the Art Review and Bibliography*, BHRA Fluid Engineering Series Vol. 3, Cotswald Press, Oxford, 1977.
47. Vincent, R. K. and Hunt, G. R., Infrared reflectance from mat surfaces. *Applied Optics* 7, 53–58, 1968.
48. Williams, C. S. and O. A. Becklund, *Optics: A Short Course for Engineers*, 58-63, 1984.